ChemComm

COMMUNICATION

View Article Online
View Journal | View Issue

Check for updates

Cite this: *Chem. Commun.*, 2022, 58, 6697

Received 14th April 2022,
Accepted 18th May 2022

DOI: 10.1039/d2cc00597b

rsc.li/chemcomm

Air-stable plasmonic bubbles as a versatile three-dimensional surface-enhanced Raman scattering platform for bi-directional gas sensing†

Yong Xiang Leong, Charlynn Sher Lin Koh, Gia Chuong Phan-Quang, Emily Xi Tan, Zhao Cai Wong, Wee Liang Yew, Bao Ying Natalie Lim, Xuemei Han and Xing Yi Ling *

Open Access Article. Published on 18 maj 2022. Downloaded on 20-07-2024 14:20:45.
This article is licensed under a Creative Commons Attribution-NonCommercial 3.0 Unported Licence.

Harnessing large hotspot volumes is key for enhanced gas-phase surface-enhanced Raman scattering (SERS) sensing. Herein, we introduce versatile, air-stable 3D 'Plasmonic bubbles' with bi-directional sensing capabilities. Our Plasmonic bubbles are robust, afford strong and homogenous SERS signals, and can swiftly detect both encapsulated and surrounding 4-methylbenzenethiol vapors.

Three-dimensional (3D) surface-enhanced Raman scattering (SERS) platforms offer tremendous potential in the detection of gaseous analytes due to the presence of micrometer-scale hotspot volumes, which allow complete utilization of the laser collection volume for maximum signal enhancement.[1,2] This, coupled with the potential for omnidirectional laser irradiation, is superior to conventional 2D SERS platforms when harnessing molecule-specific fingerprint signals from highly diffuse molecules in the gas-phase.[3] Currently, top-down lithographic approaches such as electron beam lithography produce 3D SERS platforms with immaculate features but require long processing time and high operational costs.[4] On the other hand, self-assembly of colloidal nanoparticles into extensive and compact supercrystals may inhibit effective analyte penetration and SERS signal collection from the internal regions.[5] To address this, plasmonic liquid marbles and plasmonic colloidosomes have been developed for sensing at the liquid-liquid interface, where emulsified microdroplets are encapsulated with a thin but extended network of plasmonic nanoparticles which act as substrate-less 3D SERS platforms.[6,7] While this concept has been extended to accommodate gaseous analytes through the formation of aerosolized plasmonic colloidosomes, they tend to be transient.[3] Consequently, there is still a need to design simple fabrication techniques to rapidly create air-stable 3D SERS platforms tailored for gas-phase molecular sensing.

Herein, we introduce a swift and easy method to create 'Plasmonic bubbles', which function as a versatile, air-stable 3D SERS platform with bi-directional gas sensing capabilities and provide significant analytical enhancement of 2.5×10^{10}. Inspired by the childhood bubble blower, a Plasmonic bubble can be formed by gently passing a stream of gas through a modified bubble film created using our customized formulation comprising Ag nanocubes in an aqueous solution with sodium dodecyl sulfate (SDS), gellan gum and glycerol (Scheme 1). We demonstrate the importance of each component in maintaining the structural integrity of the Plasmonic bubble, allowing it to remain air-stable for up to 7 days, which is 20 000-fold longer than a typical air bubble. By tuning the packing density, we achieve a bubble film that is compact with Ag nanocubes to give strong and homogenous SERS signals across both the x–y and x–z plane and detect methylene blue (MB) down to 10^{-10} M. The Plasmonic bubble demonstrates homogenous SERS signals and high tolerance to laser misalignment, both of which are crucial in attaining reproducible signals during measurement. Importantly, we realize bi-directional analyte sensing across the bubble film, with comparable SERS signals when exposed to gaseous 4-methylbenzenethiol (MBT) from the bubble interior and exterior. Collectively, the relative ease of fabrication, low-cost and robust nature of the Plasmonic bubble greatly boosts its

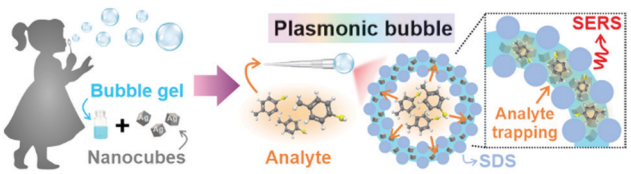

Scheme 1 Inspired by the childhood bubble blower, a Plasmonic bubble is formed by the addition of Ag nanocubes into a judiciously modified bubble gel.

Division of Chemistry and Biological Chemistry, School of Physical and Mathematical Sciences, Nanyang Technological University, Singapore 637371, Singapore. E-mail: xyling@ntu.edu.sg

† Electronic supplementary information (ESI) available. See DOI: https://doi.org/10.1039/d2cc00597b

Open Access Article. Published on 18 maj 2022. Downloaded on 20-07-2024 14:20:45.
This article is licensed under a Creative Commons Attribution-NonCommercial 3.0 Unported Licence.

applicability as a practical 3D SERS-based gas sensor, which is exceptionally useful for biomedical and environmental applications.

To fabricate the Plasmonic bubble, we first synthesize Ag nanocubes (edge length = 117 ± 6 nm), which demonstrate strong electromagnetic enhancement at the sharp cube edges and allow intense inter-cube plasmonic coupling (Fig. S1, ESI†).[8,9] The synthesized nanocubes were functionalized with 1*H*,1*H*,2*H*,2*H*-perfluorodecanethiol (PFDT) to imbue surface hydrophobicity and remove capping agents before being added to a judiciously modified bubble gel mixture which comprises water, SDS, gellan gum and glycerol.[10] Importantly, SDS and glycerol are critical in lowering the surface tension of water and stabilizing the bubble film at the air-liquid interface.[11,12] Also, glycerol and gellan gum provide a cumulative increase in dynamic viscosity, creating a set gel under room conditions.[12,13] Prior to bubble formation, the gel mixture is heated to 80 °C to lower its dynamic viscosity, allowing gradual expansion of the aqueous film into a 3D Plasmonic bubble as a stream of gas is passed through (Fig. 1A). The amount of gas can be carefully controlled to create Plasmonic bubbles of a desired size. The dynamic viscosity is regained as the temperature lowers, accelerated by the increase in surface area of the bubble film. High dynamic viscosity reduces the drainage and evaporation of the aqueous layer, allowing the Plasmonic bubble to remain air-stable while retarding the diffusion of gases across the bubble film.[14] We demonstrate that an optimized combination of 2% w/v SDS, 2% w/v gellan gum and 10% w/v glycerol allows the formation of a Plasmonic bubble that is stable for up to 7 days, which is 20 000-fold longer than a typical air bubble (Table S1, ESI†). The enhanced stability is key to ensuring that the bubble film can withstand laser irradiation during SERS measurements without rupturing.

To investigate the effect of increasing Ag nanocube concentration on the particle density within the bubble film, we create Plasmonic bubbles with five different Ag concentrations (0, 5, 20, 100, 250 mg mL^{-1}). All Plasmonic bubbles were inflated with approximately 1 cm^3 of nitrogen gas to attain a diameter of 0.6 cm (Fig. 1B). From the digital images, we observe a distinct increase in opacity of the Plasmonic bubble as the nanocube concentration increases, reflecting an increase in particle density across the bubble film. Next, we conduct scanning electron microscopy (SEM) analysis of the bubble surface and bubble film cross-section using the freeze-fracture technique to corroborate our experimental observations (Fig. 1C–E, Materials and methods). From the SEM images, we affirm that there is an increase in nanoparticle packing density from 7 to 58 particles per μm^2 with an increase in Ag nanocube concentration added (Fig. 1E). This increase in particle density adheres to a strong sigmoidal relationship, with a low reduced chi-square (red χ^2) value of 0.09 and a coefficient of determination (R^2) of 0.98 (Fig. 1C). The low reduced χ^2 value indicates excellent goodness-of-fit, while an R^2 of close to 1 describes good replicability of the observed particle densities using the sigmoidal function. At a Ag concentration of 250 mg mL^{-1}, the surface coverage by Ag nanocubes in the Plasmonic bubble film is estimated to be 79%

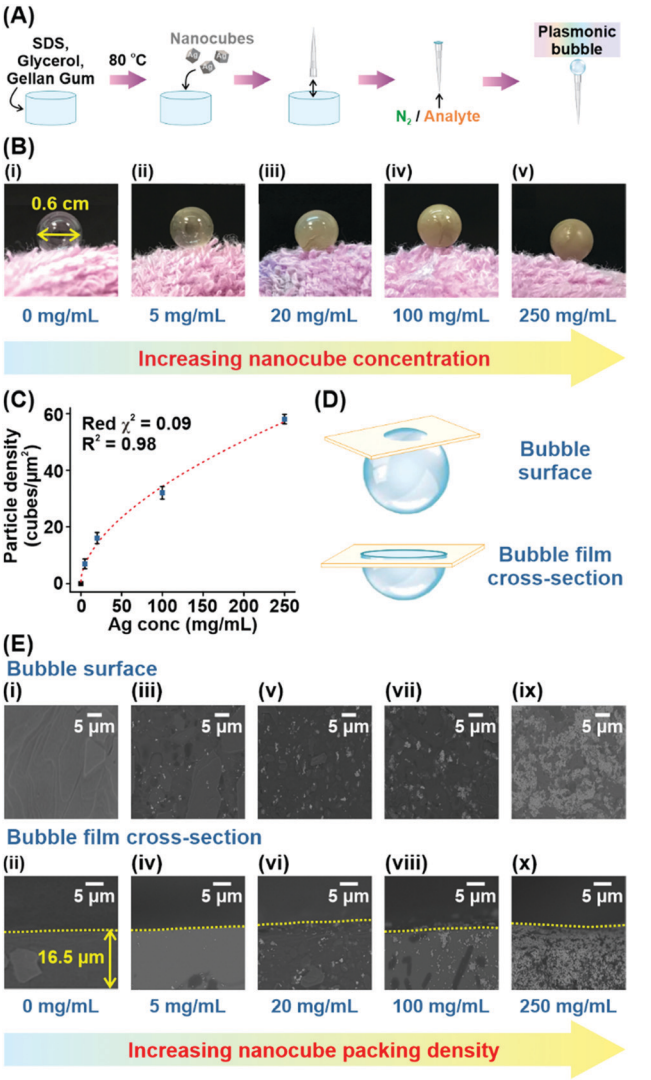

Fig. 1 (A) Formation of a Plasmonic bubble. (B) Plasmonic bubble with varying Ag nanocube concentrations (mg mL^{-1}): (i) 0, (ii) 5, (iii) 20, (iv) 100 and (v) 250. (C) Relationship between nanocube concentration and packing density in the bubble film. (D) The bubble surface and bubble film cross-section. (E) SEM images for Ag nanocube concentrations (mg mL^{-1}): (i and ii) 5, (iii and iv) 20, (v and vi) 100 and (vii and viii) 250.

(Supplementary note 1, ESI†). From the sigmoidal relationship, we deduce that a further increase in Ag concentration will result in diminishing increase in packing densities as the nanocubes cannot form perfectly compact structures within the 3D bubble film. In fact, a further increase in packing density is not ideal as the large amount of Ag would hinder laser penetration as well as make the platform particle inefficient.[15] Finally, we note that the Plasmonic bubbles show a consistent film thickness of 16.5 ± 0.5 μm as averaged over five distinct bubble measurements (Table S2, ESI†).

Using MB as a model analyte, we investigate the SERS performance of the Plasmonic bubble embedded with different amounts of Ag nanocubes. The intense aromatic C=C ring stretching mode of MB at 1633 cm^{-1} serves as a stable reference peak to compare the relative analytical enhancements at

 This journal is © The Royal Society of Chemistry 2022

Open Access Article. Published on 18 maj 2022. Downloaded on 20-07-2024 14:20:45.
This article is licensed under a Creative Commons Attribution-NonCommercial 3.0 Unported Licence.

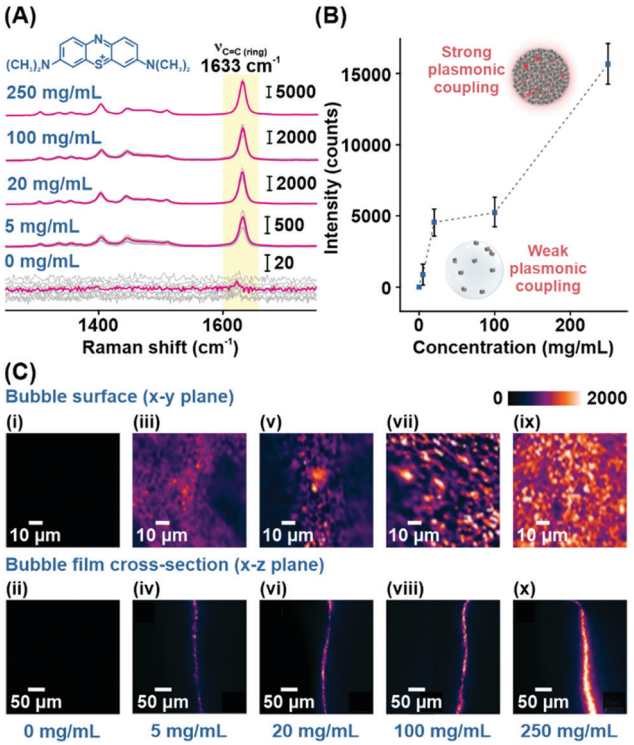

Fig. 2 (A) SERS spectra of MB added to the Plasmonic bubble film with varying nanocube concentrations. (B) Signal intensity of the 1633 cm^{-1} peak. (C) Hyperspectral SERS map for increasing Ag concentrations (mg mL^{-1}): (i and ii) 5, (iii and iv) 20, (v and vi) 100 and (vii and viii) 250.

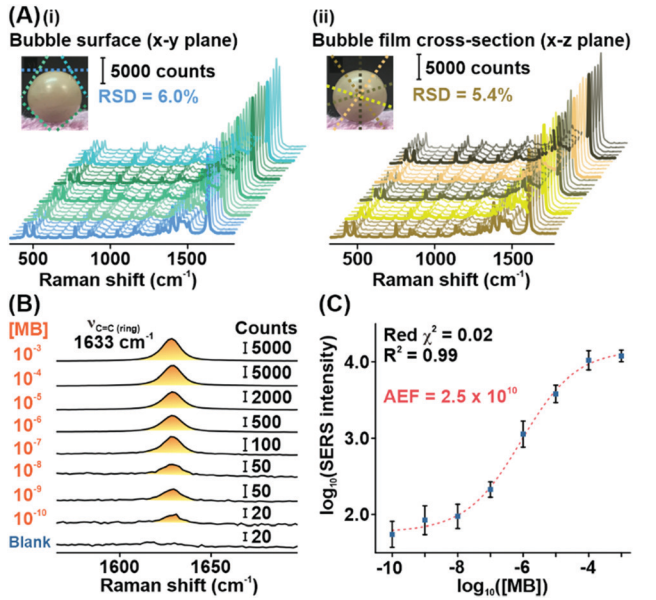

Fig. 3 (A) SERS spectra showing high signal homogeneity across different laser irradiation angles along the (i) bubble surface and (ii) bubble film cross-section. (B) SERS spectra showing the 1633 cm^{-1} peak changes with varying concentrations of MB. (C) Computing the detection limit and analytical enhancement factor of the Plasmonic bubble using the 1633 cm^{-1} peak.

different nanocube packing densities (Fig. 2A).[1] Without Ag nanocubes, MB Raman signals cannot be detected due to the inherently weak Raman scattering in the absence of plasmonic enhancement. As the nanocube concentration increases from 5 to 250 mg mL^{-1}, the packing density increases, creating significant inter-cube plasmonic coupling, which boosts the SERS signals by about 20-fold from 882 to 15 653 counts (Fig. 2B and Table S3, ESI†). The effect of plasmonic coupling can be clearly observed through hyperspectral SERS mapping of the acquired analyte signals across both the bubble surface (x–y plane) and the bubble film cross-section (x–z plane) (Fig. 2C). At a Ag concentration of 250 mg mL^{-1}, the x–y plane SERS map is uniformly filled with regions of strong plasmonic activity, indicating homogenous distribution of densely packed Ag nanocubes within the bubble film (Fig. 2Cix). Similarly, the x–z plane SERS map shows strong plasmonic activity concentrated within the bubble film, signifying effective laser penetration across the entire thickness of the film (Fig. 2Cx). Achieving this is critical to ensure maximal enhancement of the SERS signals and good signal reproducibility when utilizing the Plasmonic bubble as a sensor for gaseous analytes. Henceforth, all Plasmonic bubbles are fabricated with the addition of 250 mg mL^{-1} Ag nanocubes and inflated using approximately 1 cm^3 of gas, unless otherwise stated.

Subsequently, we demonstrate the excellent signal consistency of the Plasmonic bubble with different directions of laser irradiation (Fig. 3A). 25 unique SERS spectra were acquired with the Plasmonic bubble in the x–y (bubble surface) and x–z (bubble film cross-section) planes by varying the angle of laser irradiation slightly with each acquisition. Using the MB reference peak, the relative signal standard deviation for SERS spectra across the bubble surface and bubble film cross-section is 5.4% and 6.0%, respectively. The relatively low signal standard deviation signifies that the Plasmonic bubble has high tolerance to laser misalignment, which is crucial in practice where slight deviations occur during sample measurements. Notably, the high signal consistency also explicates the robustness of the Plasmonic bubble even with repeated laser irradiation.

To quantify its sensing efficiency, we assess the detection limit of the Plasmonic bubble by adding decreasing concentrations of MB into the bubble gel. We demonstrate that the Plasmonic bubble can detect MB down to 10^{-10} M, which corresponds to an analytical enhancement factor of 2.5×10^{10} (Fig. 3B, Supplementary note 2, ESI†). The MB reference peak exhibits a strong sigmoidal relationship from 10^{-3} to 10^{-10} M, with a low reduced χ^2 value of 0.02 and excellent R^2 of 0.99 (Fig. 3C). The sigmoidal relationship between the MB concentration and SERS signal intensity afforded by the Plasmonic bubble signifies a unique advantage in acquiring relatively stronger signals at low analyte concentrations, which is crucial for the detection of diffuse gaseous analytes (Supplementary note 3, ESI†).

As a proof of concept, we demonstrate the ability of the Plasmonic bubble to achieve bi-directional gas sensing using saturated MBT vapor (vapor pressure = 0.807 mmHg) (Fig. 4A, Materials and methods). Specifically, bi-directional sensing

Open Access Article. Published on 18 maj 2022. Downloaded on 20-07-2024 14:20:45.
This article is licensed under a Creative Commons Attribution-NonCommercial 3.0 Unported Licence.

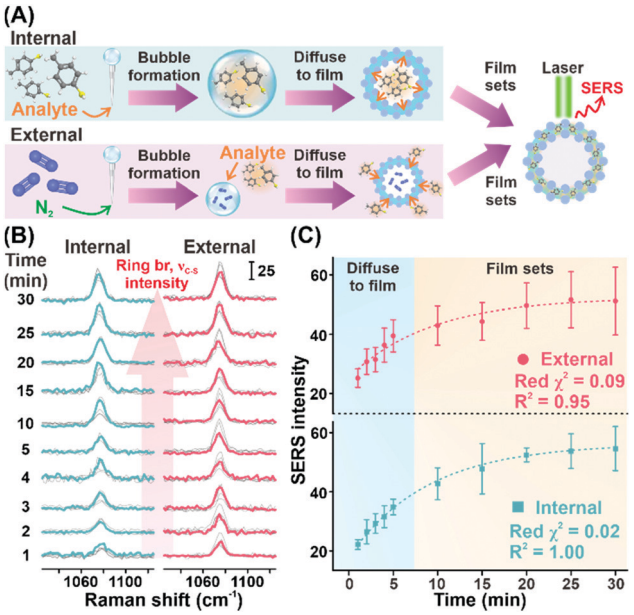

Fig. 4 (A) Two different modes of gas sensing. (B) Time-dependent SERS spectra of MBT show the increase in the intensity of the 1077 cm^{-1} peak. (C) Comparing the SERS signal intensity of MBT using two different modes of analyte sensing.

refers to the ability to detect MBT vapor that is encapsulated within the Plasmonic bubble (referred to as internal) as well as external MBT vapor that is exposed to the Plasmonic bubble surface (referred to as external). For both configurations, we observe a strong and distinct peak at 1077 cm^{-1}, which is characteristic of the concurrent ring breathing and C–S stretching vibrational mode of MBT (Fig. 4B).[1]

We further conduct a temporal study to study the diffusion mechanism in each configuration. In general, we observe an increase in SERS signal intensity with time for the first 30 minutes of MBT exposure, which translates to diffusion of MBT vapor into the Plasmonic bubble film from the bubble interior and exterior, respectively (Fig. 4C). In both cases, we observe a sharp increase in SERS signal intensity in the first 5 minutes, which correlates to rapid diffusion of MBT molecules into the plasmonically active aqueous film of the Plasmonic bubble in accordance with Fick's law.[16] After which, the rate of increase in SERS signal intensity is slowed down and plateaus at about 20 minutes. Importantly, the increase in signal intensity shows an exponential relationship with excellent reduced χ^2 and R^2 values for both internal and external configurations (internal: red χ^2 = 0.02, R^2 = 1.00; external: red χ^2 = 0.09, R^2 = 0.95) (Fig. 4C). Also, the relatively constant signal intensity from 20 to 30 minutes upon exposure to MBT signifies the ability of the Plasmonic bubble to trap gaseous analytes within the bubble film as it sets, avoiding signal loss over time and potential interferences from external sources. Moreover, both the internal and external configurations show comparable trends for the MBT SERS signal intensity, indicating the versatility of the Plasmonic bubble and the potential for multiplex gas sensing.

In conclusion, we showcase our design of a versatile, air-stable centimeter-sized 3D Plasmonic bubble with bi-directional gas sensing capabilities, strong SERS analytical enhancement of 2.5 × 10^{10} and a low limit of detection of 10^{-10} M. With an internal volume of approximately 1 cm^3 and diameter of 0.6 cm, a Ag concentration of 250 mg mL^{-1} creates a densely packed bubble film with highly homogenous and reproducible SERS signals and strong tolerance to laser misalignment. Notably, unlike conventional air bubbles, the Plasmonic bubble can retain its structural integrity for an extended period of 7 days due to high dynamic viscosity of the aqueous layer. The high stability permits laser irradiation for SERS measurements with ease without any risk of disrupting the bubble structure. Finally, the ability to conduct bi-directional gas sensing from the bubble interior and exterior imbues significant flexibility to the Plasmonic bubble as a 3D SERS platform for easy integration with various biomedical and environmental applications.

Conflicts of interest

The authors declare no conflict of interest.

Notes and references

1 G. C. Phan-Quang, N. Yang, H. K. Lee, H. Y.-F. Sim, C. S.-L. Koh, Y.-C. Kao, Z. C. Wong, E. K.-M. Tan, Y.-E. Miao, W. Fan, T. Liu, I. Y. Phang and X. Y. Ling, *ACS Nano*, 2019, **13**(10), 12090–12099.
2 G. C. Phan-Quang, X. Han, C. S.-L. Koh, H. Y.-F. Sim, C. L. Lay, S. X. Leong, Y. H. Lee, N. Pazos-Perez, R. A. Alvarez-Puebla and X. Y. Ling, *Acc. Chem. Res.*, 2019, **52**(7), 1844–1854.
3 G. C. Phan-Quang, H. K. Lee, H. W. Teng, C. S.-L. Koh, B. Q. Yim, E. K.-M. Tan, W. L. Tok, I. Y. Phang and X. Y. Ling, *Angew. Chem., Int. Ed.*, 2018, **57**(20), 5792–5796.
4 S. Kasani, K. Curtin and N. Wu, *Nanophotonics*, 2019, **8**(12), 2065–2089.
5 M. Chen, I. Y. Phang, M. R. Lee, J. K.-W. Yang and X. Y. Ling, *Langmuir*, 2013, **29**(23), 7061–7069.
6 G. C. Phan-Quang, H. K. Lee, I. Y. Phang and X. Y. Ling, *Angew. Chem., Int. Ed.*, 2015, **54**(33), 9691–9695.
7 X. Han, C. S.-L. Koh, H. K. Lee, W. S. Chew and X. Y. Ling, *ACS Appl. Mater. Interfaces*, 2017, **9**(45), 39635–39640.
8 C. S.-L. Koh, H. K. Lee, X. Han, H. Y.-F. Sim and X. Y. Ling, *Chem. Commun.*, 2018, **54**(20), 2546–2549.
9 Y. X. Leong, Y. H. Lee, C. S.-L. Koh, G. C. Phan-Quang, X. Han, I. Y. Phang and X. Y. Ling, *Nano Lett.*, 2021, **21**(6), 2642–2649.
10 H. Mao, J. Feng, X. Ma, C. Wu and X. Zhao, *J. Nanopart. Res.*, 2012, **14**(6), 887.
11 C. C. Ruiz, L. Díaz-López and J. Aguiar, *J. Dispers. Sci. Technol.*, 2008, **29**(2), 266–273.
12 N.-S. Cheng, *Ind. Eng. Chem. Res.*, 2008, **47**(9), 3285–3288.
13 M. C. García, M. C. Alfaro, N. Calero and J. Muñoz, *Biochem. Eng. J.*, 2011, **55**(2), 73–81.
14 P. M. Wilkinson, A. Van Schayk, J. P.-M. Spronken and L. L. Van Dierendonck, *Chem. Eng. Sci.*, 1993, **48**(7), 1213–1226.
15 Y. Yang, Y. H. Lee, I. Y. Phang, R. Jiang, H. Y.-F. Sim, J. Wang and X. Y. Ling, *Nano Lett.*, 2016, **16**(6), 3872–3878.
16 A. Fick, *Ann. Phys.*, 1855, **170**(1), 59–86.

This journal is © The Royal Society of Chemistry 2022